International Journal of Nanomedicine

Dovepress
Taylor & Francis Group

Open Access Full Text Article

ORIGINAL RESEARCH

Unveiling Theranostics: Nanocomplex-Assisted Photodynamic Eradication of Aggressive Cancer Cells and Modulation of Tumor-Associated Macrophages

Austeja Butkute[1,2,*], Evelina Kazlauske[3,4,*], Agata Mlynska[1,4], Emile Peciukaityte[3], Vitalijus Karabanovas[3,4], Ricardas Rotomskis[3,5], Simona Steponkiene[3]

[1]Laboratory of Immunology, National Cancer Institute, Vilnius, Lithuania; [2]Life Science Center, Vilnius University, Vilnius, Lithuania; [3]Biomedical Physics Laboratory of National Cancer Institute, Vilnius, Lithuania; [4]Department of Chemistry and Bioengineering, Vilnius Gediminas Technical University, Vilnius, Lithuania; [5]Biophotonics Group of Laser Research Center, Vilnius University, Vilnius, Lithuania

*These authors contributed equally to this work

Correspondence: Simona Steponkiene, Biomedical Physics Laboratory of National Cancer Institute Vilnius, Vilnius, Lithuania, Email simona.steponkiene@nvi.lt

Background: Photodynamic therapy (PDT) is a promising tool that utilizes photosensitizers (PS) for two functions: cancer imaging by fluorescence (diagnostics), and treatment by the generation of reactive oxygen species (therapy). Despite its theranostic approach, the efficacy of PDT is often hampered by limited penetration of light into tissues, tumor heterogeneity, and the immunosuppressive tumor microenvironment (TME). Moreover, diagnostics and treatment are activated simultaneously, without the possibility of switching between two processes.

Methods: We used photosensitizer chlorin e6 (Ce6) and luminescent quantum dots (QDs) to create a theranostic nanocomplex. Two different light sources were used (980 nm or 650 nm light) to activate either the photoluminescence of quantum dots (QDs) or the generation of singlet oxygen by Ce6. Four distinct CRC cell lines were utilized to represent tumor heterogeneity. The therapeutic efficacy of nanocomplex was assessed in CRC and tumor-associated macrophages (TAMs), a key component of the immunosuppressive TME. Immunomodulatory effects were explored by exposing resident and recruited TAM models to a conditioned medium from PDT-treated CRC cells, followed by gene expression analysis.

Results: Spectral characterization of the QDs-Ce6 nanocomplex demonstrated selective switching between diagnostic and therapeutic modes. Two-photon absorption was activated in QDs by 980 nm laser, thus broadening its excitation capabilities into the infrared region. The nanocomplex accumulated efficiently and uniformly across all CRC cell lines, regardless of their aggressiveness or drug sensitivity. The effect of nanocomplex-assisted PDT was the same among CRC cell lines, contrasting with the variable sensitivity to 5-fluorouracil. Additionally, the PDT caused M2 macrophages to lose their pro-tumor characteristics while potentiating their ability to present antigens. Additionally, M0 macrophages displayed a reduction in immunosuppressive signaling.

Conclusion: The QDs-Ce6 nanocomplex exhibits robust photodynamic cytotoxicity and immunomodulatory potential. These findings highlight the potential of nanocomplex for targeting the aggressive type of tumor cells and the TAM.

Keywords: nanocomplex, immune cells, tumor microenvironment, photosensitizer, quantum dots, two-photon absorption

Introduction

Photodynamic therapy (PDT) is a medical treatment that uses light-sensitive compounds called photosensitizers (PS), which are activated by a specific wavelength of light to produce a therapeutic effect by the generation of reactive oxygen species (ROS).[1] In the absence of light, PS has no toxicity. Upon absorbing light of a suitable wavelength, PS molecules trigger photocytotoxic effects localized to the region of their presence. Moreover, once excited by light, PS molecules emit fluorescence. However, ROS and fluorescence occur simultaneously without possibly switching between the two

Received: 17 January 2025
Accepted: 25 June 2025
Published: 8 August 2025

Graphical Abstract

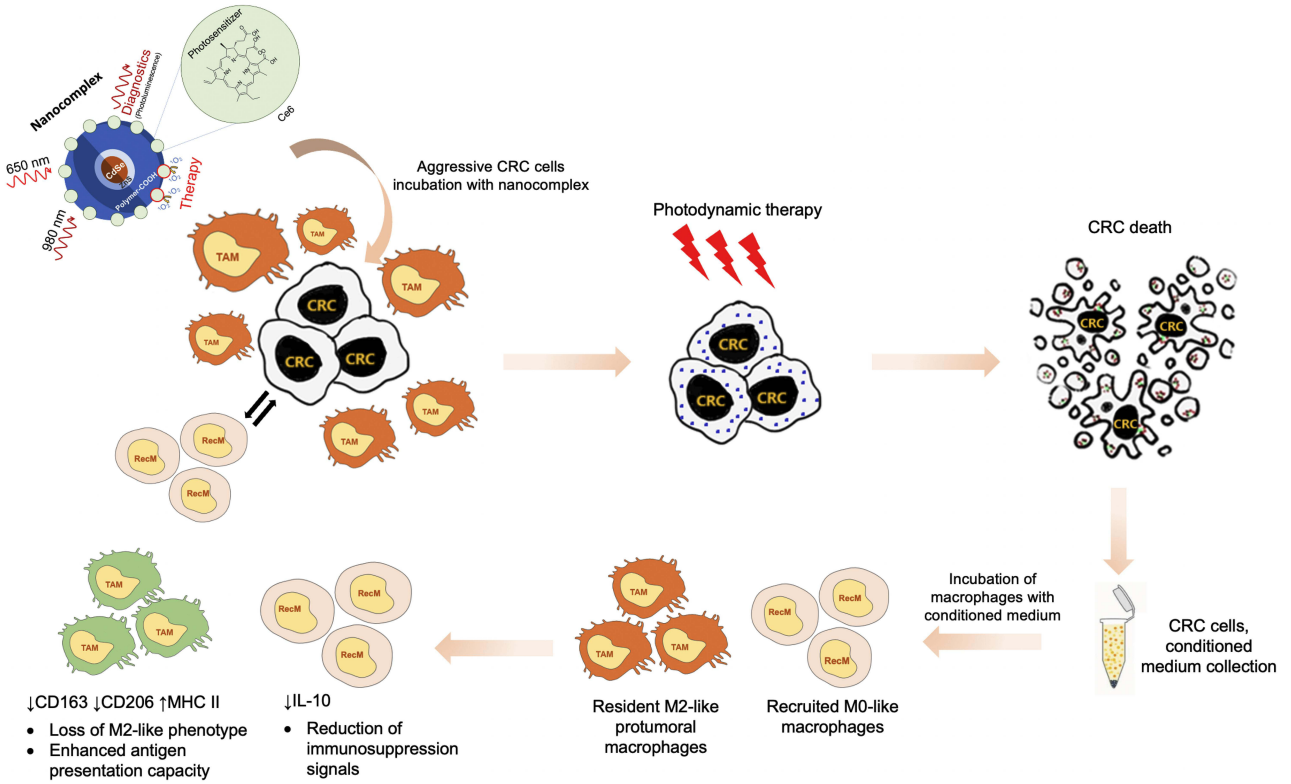

processes.[2] In recent years, the diagnostics and therapeutic functions of PS have been separated to act on the demand of two different switchers using versatile nanotechnology platforms.[3,4]

Multiple nanomedicines have been evaluated over the years with different diagnostic and therapeutic properties, utilized by combining metal core and adding functional ligands or therapeutic molecules.[5] One example of a nanocomplex extensively used in biomedical research is the quantum dots (QDs) and PS chlorin e6 (Ce6) nanocomplex.[6] QDs are nanocrystals characterized by sharp photoluminescence (PL) bands, high PL quantum yield, resistance to fading, and versatile surface modification capabilities compared to classical fluorescent dyes. Ce6, a second-generation PS with a high extinction coefficient, has already been applied clinically and is known as Photolon®.[7,8] Since QDs are not efficient generators of ROS, which is crucial for inducing tumor cell death during PDT, their combination with Ce6 enables the QDs-Ce6 to gain PDT properties and successfully eradicate cancer cells.[9] The highly photostable PL of QDs is suitable for cancer diagnostics and tracking of nanocomplex in vivo.[10] However, the QDs-Ce6 complex is excited at the UV-VIS region, which limits its accessibility to deeper tissues. The tissue transparency window for efficient light penetration, also known as the tissue optical window, is considered to range from 600 nm to 1300 nm.[11] Recently, two-photon absorption (TPA) compounds have emerged as a highly promising tool for fluorescence imaging.[12] TPA involves the simultaneous absorption of two photons (TP), effectively halving the energy per photon and doubling the wavelength. QDs possess a large TPA cross-section,[13] which could serve for diagnostics, while the near-infrared absorption properties of Ce6 could serve as an effective sensitizer.

Colorectal cancer (CRC) is among the most heterogeneous cancer types, posing a major challenge to effective treatment. The factors contributing to intratumoral CRC heterogeneity are often cell-intrinsic, such as mutational status, microsatellite instability, and stemness-related transcriptional profile.[14] These intrinsic factors are associated with the aggressive behavior of cancer cells,[15] including high invasiveness, pronounced stemness properties, resistance to

treatment, and adaptation to diverse microenvironmental conditions. However, the CRC heterogeneity can also arise from the host immune response and manifest as distinct inflammatory microenvironment profiles.[16] Within the tumor microenvironment (TME) of CRC, tumor-associated macrophages (TAMs) have been found to be the most abundant group of tumor-infiltrating immune cells.[17,18] While the mechanisms underlying the interactions between CRC and TAMs are complex, it is agreed that cancer progression or response to therapy depends on the nature of the polarization of TAMs, with M1 being tumor-suppressive and M2 being tumor-promoting.[19]

In the context of PDT, TAMs can be activated by ROS generated during treatment. Activated TAMs can secrete cytokines (eg TNF-α, IL-1β, IL-6, and IL-8) and signaling molecules that attract other immune cells to help destroy cancer cells. However, TAMs may also play a role in limiting the efficacy of PDT. Some studies have shown that TAMs can protect cancer cells from the effects of PDT by producing factors that reduce ROS production or by taking up and removing PS that accumulates in cancer cells.[20] Key challenges in using PDT for direct or indirect targeting of TAMs include developing novel multimodal nanomedicines and validating their immunomodulatory effects.[21] Addressing this task is crucial to understanding the underlying mechanisms of TAM response to PDT, enhancing its antitumoral effect, and accelerating the clinical translation of this approach.

This study explored a multifunctional QDs-Ce6 nanocomplex designed to separate diagnostic and therapeutic functionalities, using 980 nm light for TPA excitation of QDs and 650 nm light for PDT by Ce6. This represents a novel approach, potentiating the nanocomplex by infrared light and enabling deeper tissue penetration. Accumulation, biocompatibility, and PDT efficacy of QDs-Ce6 nanocomplex was tested in a panel of molecularly and functionally different CRC cancer cell lines. Our findings highlight that while CRC cells exhibit substantial heterogeneity in aggressiveness and drug sensitivity, the QDs-Ce6 nanocomplex accumulates uniformly across all examined cells and demonstrates consistent PDT efficacy, overcoming limitations of chemotherapy. Furthermore, we provide evidence for the immunomodulatory potential of nanocomplex-induced PDT, showing that conditioned media from treated CRC cells, especially the aggressive cell line, modulates M2-like TAMs into a more immunostimulatory phenotype, including upregulation of antigen presentation marker and downregulation of immunosuppressive markers. By integrating nanotechnologies with immunomodulatory strategies, our study lays the groundwork for innovative approaches targeting cancer cells and their surrounding microenvironment.

Materials and Methods

Materials

The study utilized commercially available carboxyl-functionalized QDs (Qdot 625 ITK, Invitrogen, Thermo Fisher Scientific, Waltham, MA, USA) with a PL wavelength peak of 625 nm and photosensitizer chlorin e6 (Ce6). QDs are made of a semiconductor core composed of CdSe and a layer of ZnS, combined with a polymer coating that includes carboxyl surface groups. The average size of the QDs used in this study is approx. 15 nm, ζ potential is −20 mV as indicated by the manufacturer[22] and in other publications.[23] Ce6 (Frontier Scientific Inc, Newark, DE, USA) was prepared as a stock solution in a small volume as follows: Ce6 powder was diluted in 0.2 M NaOH, followed by further dilution of phosphate buffer (PB, 0.1 M, pH = 7.0, containing 0.057 M Na_2HPO_4 and 0.042 M $NaHPO_4$). The extinction coefficient of Ce6 at 405 nm is ε = 175 000 M^{-1} cm^{-1} as reported in the publication by Dapkute et al.[10] Singlet Oxygen Sensor Green (SOSG) (Thermo Fisher Scientific, Waltham, USA), a commercially available fluorescent sensor, was used for singlet oxygen detection with no noticeable reaction to hydroxyl radicals or superoxide.[24]

Cell Culture

Human CRC cell lines LS1034, SW620, HCT116, and DLD1 were obtained from the American Type Culture Collection (ATCC, Manassas, VA, USA). These adherent cell lines were grown in RPMI-1640 supplemented with 10% fetal bovine serum (FBS, Thermo Fisher Scientific, USA) and 1% antibiotics 100 U/mL penicillin and 100 μg/mL streptomycin (Thermo Fisher Scientific, USA). Cells were passaged after they reached 70% confluency.

The human leukemic monocyte cell line THP-1 was obtained from the American Type Culture Collection (ATCC, USA) and grown in RPMI-1640 supplemented with 10% FBS. THP-1 cells were cultured in a complete RPMI-1640 cell

culture medium and routinely passaged to maintain a suspension concentration of 2×10^5 cells/mL to 1×10^6 cells/mL. Cells were maintained at 37 °C in a humidified atmosphere at 5% CO_2 during all experiments.

Clonogenic Assay

CRC cell lines LS1034, SW620, HCT116, and DLD1 were seeded in 6-well plates with 200 cells per well in RPMI-1640 medium and allowed to form colonies. After 7 days, cells were fixed (70% EtOH for 10 min, then 96% EtOH solution for 10 min) and stained with 0.2% crystal violet (Sigma-Aldrich, St, Louis, MO USA) for 15 min. The plates were washed with water and dried. Emergent colonies (>50 cells) were counted, and colony formation efficiency (CFE) was estimated according to the equation (1):

$$CFE = \frac{number\ of\ colonies}{number\ of\ cells\ seeded} \times 100\% \quad (1)$$

Expression of Surface Markers

To evaluate the surface phenotype, cancer cells were detached, counted, and distributed into cytometric tubes at 1 million cells per tube. The cells were washed with PBS and centrifuged at 300g for 5 minutes. After removing the supernatant, single staining was performed by incubating the cell pellets with the following antibodies for 20 minutes in the dark at 4°C: 1 µL anti-CD133-PE (Miltenyi Biotec, Bergisch Gladbach, Germany), 1 µL anti-CD44-APC (Miltenyi Biotec, Germany), 1 µL anti-ESA-APC (BD Biosciences, Franklin Lakes, NJ, USA), 4 µL anti-MHCI-FITC (BD Biosciences, USA), and 2 µL anti-PD-L1 (BD Biosciences, USA). After staining, the cells were washed twice with PBS, resuspended in 200 µL PBS, and analyzed using a BD Biosciences LSR II flow cytometer. Data from at least 10,000 events per sample were processed with FACSDiva software.

Wound Healing Assay

CRC cell lines were seeded in a 24-well plate at densities specific to each line: HCT116 and DLD1 at 3.5×10^5 cells/mL, and LS1034 and SW620 at 4×10^5 cells/mL. The cells were then allowed to grow and proliferate for 48 hours to form a confluent monolayer. For the wound healing assay, the gap between cells was created by scratching the cell monolayer with a sterile 200 µL pipette tip. Cells were photographed from the moment of wound formation and after 24 hours. Migration dynamics was evaluated using the ImageJ 1.49a software (NIH, Bethesda, MD, USA).

QDs-Ce6 Nanocomplex Preparation and Stability Studies

QDs-Ce6 complex (hereinafter referred to as "nanocomplex") is formed by mixing QDs and Ce6. The molar ratios of QDs and Ce6 for the nanocomplex preparation were adopted from our previous studies[9] and maintained throughout the whole study at 1:100 molar ratio. The nanocomplex was prepared by a droplet formation scheme: the required amount of Ce6 for the experiment was added to a tube, mixed with QDs, and allowed to sit for 2 min to facilitate rapid complex formation. Further measurements were performed by diluting the nanocomplex with the desired medium. For spectral measurements, the concentration of QDs-Ce6 was 5 nM, (1:100 molar ratio), the final medium was RPMI-1640 ((Roswell Park Memorial Institute (RPMI) 1640 medium, Thermo Fisher Scientific, USA, without phenol red). For QDs-Ce6 nanocomplex stability studies in cell culture medium over time (up to 24 hours), the concentration of QDs-Ce6 was 16 nM, identical to the concentration of nanocomplex used for all cell culture experiments. During all studies, the nanocomplex was prepared in a serum-free environment.

Singlet Oxygen Production

SOSG was prepared according to the manufacturer's protocol. QDs (8 nM), QDs-Ce6 (8 nM, 1:100), Ce6 (800 nM) samples were dispersed in RPMI-1640 medium, and, subsequently, SOSG was added, resulting in a 0.005 mM SOSG reagent concentration per sample. To induce the generation of singlet oxygen, samples were irradiated using a xenon light source MAX-302 (Asahi Spectra, Tokyo, Japan) with a 650/70 nm bandpass filter from 2 s up to 360 s (t), to achieve

light irradiation doses comparable to the ones used on the cells (0–30 J/cm^2). During irradiation experiments, samples were constantly mixed with a magnetic stirrer.

The fluorescence of the SOSG reagent was measured by the Edinburgh Instruments FLS980 spectrometer (λ_{ex}=504 nm) (Edinburgh Instruments, Livingston, UK). For each time point, an integrated fluorescence intensity was calculated using equation (2):

$$I_{SOSG} = \int_{525}^{535} Id\lambda \tag{2}$$

I_{SOSG} represents the area under the curve for fluorescence intensity between λ_{525} and λ_{535}.

The increase in fluorescence intensity of the SOSG due to singlet oxygen production, activated by irradiation, was determined by mathematically subtracting the background fluorescence intensity of SOSG at a given time point t [2;360] s of irradiation, calculated by equation (3):

$$\Delta I_{SOSG} = I_{SOSG(t)} - I_{SOSG(t0)} \tag{3}$$

ΔI_{SOSG} – represents the change in fluorescence signal of SOSG due to light exposure. It is proportional to the concentration of singlet oxygen.[24]

Two-Photon Excitation Studies

Two-photon (TP) excitation of QDs-Ce6 (1:100) samples was induced by PSU-III-LED (Edinburgh Instruments, Livingston, UK) laser operating at 980 nm wavelength with continuous mode. The average max laser power of focused beam entering the sample was approximately 1.5 W. To measure a power-dependent TP-excitation characteristics, power of a laser was regulated by changing the current with a knob located at the laser block. Diameter of a beam entering sample was approximately 0.6 mm. TP induced photoluminescence signal of QDs was collected by the Edinburgh Instruments spectrometer FLS920P. The temperature of samples was controlled by PCB 1500 Water Peltier system (Agilent, Santa Clara, CA USA). All experiments were performed at 25 °C.

Confocal Microscopy of QDs-Ce6 Nanocomplex in Cells

For cellular imaging studies, cells were seeded into 8-well chambered coverglass with borosilicate glass bottom (LabTek, Nunc, Thermo Fisher Scientific, Roskilde, Denmark) at a density of 5×10^4 cells/chamber and incubated for 24 hours at standard culture conditions. To evaluate the nanocomplex accumulation, cells were washed with phosphate buffered saline (PBS, Gibco, Thermo Fisher Scientific, USA) and treated with RPMI-1640 containing QDs-Ce6 nanocomplex (16 nM QDs and 1600 nM of Ce6 (molar ratio 1:100)) for 24 hours. 15 min till the end of the incubation, the cells nuclei were stained with Hoechst 33258 dye. Afterward, the old medium was gently aspirated, the cells were washed four times with Dulbecco's PBS (DPBS, without Ca^{2+} and Mg^{2+}), and a complete cell growth medium was added. Cells were imaged with laser scanning confocal microscope Nikon Eclipse TE2000 C1si equipped with 405 nm and 488 lasers and 60x NA 1.4 oil immersion objective (Nikon, Tokyo, Japan). To maintain the standard culture conditions (37º temperature, 5% CO2) during microscopy imaging, a CO_2 microscope stage incubation system (OkoLab, Naples, Italy) was used. The fluorescence of visualized components was detected using bandpass filters as follows: Hoechst with 450/17, Ce6 and QDs-Ce6 complex with 605/75. A separate detection unit was equipped for spectral imaging. A 32-channel detection system registered a spectral range of 550–750 nm for each given pixel of micrographs. Regions of interest were selected to analyze the photoluminescence spectra at the specific sites of intracellular space. The obtained images were processed with EZ-C1 Bronze v3.80 (Nikon, Japan) and ImageJ 1.49a (NIH, USA) software.

Cellular Uptake of QDs-Ce6 Nanocomplex by Flow Cytometry

CRC cells were seeded in a 24-well plate at a density of 7.5×10^4 cells/mL and cultured for 48 hours. The cells were treated with RPMI-1640 medium containing the QDs-Ce6 nanocomplex (molar ratio 1:100, QDs 16 nM and Ce6 1600 nM) at different time intervals (1, 3, 6, and 24 hours) before measurement. For flow cytometry, 20,000 events were collected using a BD Biosciences LSR II flow cytometer (Franklin Lakes, NJ, USA). QD- Ce6 signals were registered

using a 633 nm excitation laser and emission filter 660/20 nm. Data were analyzed using FACS Diva software (BD Biosciences, USA) and FlowJo (Ashland, OR, USA).

Biocompatibility of QDs-Ce6 Nanocomplex

CRC cells were seeded in a 96-well plate at 2×10^4 cells/mL density with a total volume of 150 µL RPMI-1640 medium. After 24 hours, nanocomplex at concentrations of 5 nm, 16 nM and 25 nM (QDs:Ce6 ratio 1:100) was added to the cells and incubated for 24 hours. To assess dark cytotoxicity, cell viability was evaluated after 24 hours of incubation with nanocomplex. A serum-free RPMI-1640 medium was used as a control. Then, CCK-8 reagent was added (10 µL per well) to each well and incubated for 1 hour. Cell cells were maintained at 37 °C in a humidified atmosphere at 5% CO_2 during all experiments. Optical density at 450 nm was measured using a microplate absorbance reader (ELx800, BioTek, Winooski, VT, USA).

PDT Effect of QDs-Ce6 Nanocomplex

CRC cells were seeded in a 96-well plate at a density of 2×10^4 cells/mL with a total volume of 150 µL in a complete growth medium. After 24 hours, the growth medium was replaced with RPMI-1640 medium containing QDs-Ce6 nanocomplex at a concentration of 16 nM (QDs:Ce6 molar ratio 1:100) and incubated for 24 hours. Afterward, the old medium was gently aspirated, the cells were washed four times with Dulbecco's PBS (DPBS, without Ca^{2+} and Mg^{2+}), and a complete cell growth medium was added. To assess photodynamic effects, cells were irradiated using xenon light source MAX-302 (Asahi Spectra, Tokyo, Japan) with 650/70 nm bandpass filter for 51.6–154.8 s for each well to achieve the irradiation dose of 10, 20, 30 J/cm^2. After irradiation, cells were placed back into the standard culture conditions for 24 hours. Then CCK-8 reagent was added (10 µL per well) to each well and incubated for 1 hour. Optical density at 450 nm was measured using a microplate absorbance reader (ELx800, BioTek, USA).

Chemotherapy Drug 5-Fluorouracil Cytotoxicity Assay

The chemotherapy effect of 5-fluorouracil (5-FU) was examined using the CCK-8 assay in CRC cell lines. CRC cell lines were seeded in 96-well plates at 1×10^4 cells/well density. After 24 hours, cells were treated with 5-FU at concentrations ranging from 0.03 µM to 200 µM. After incubation, CCK-8 reagent (Dojindo Europe, Munich, Germany) was added (10 µL per well) into each well and incubated for 1 hour. Optical density at 450 nm was measured using a microplate absorbance reader (ELx800, BioTek, USA). The treatment groups were compared with the control group, and the results were expressed as a percentage of viable cells. The drug's 50% inhibitory concentrations (IC50) were determined using a built-in non-linear regression model for dose response in GraphPad Prism 9 (La Jolla, CA, USA).

Indirect Immunomodulatory Effect of Nanocomplex-Induced PDT on Tumor-Associated Macrophages

Conditioned Medium Preparation and Macrophage Treatment

Conditioned medium was prepared using two CRC cell lines: LS1034 and DLD1. The photodynamic effect of the QDs-Ce6 complex was induced as described above with a xenon lamp irradiation to achieve a light dose of 20 J/cm^2 for each well. After irradiation, cells were placed back in the incubator for 24 hours. The conditioned medium was collected and centrifuged for 15 min at 1000 g to remove tumor cells or debris.

THP-1 cells were seeded in 6-well plate at a density of 3.5×10^5 cells/mL in RPMI-1640 medium supplemented with 20 ng/mL phorbol-12-myristate-13-acetate (PMA, Tocris Bioscience, Bristol, UK) for 48 hours, during which cells differentiate into M0 macrophages. In parallel, for M2 polarization, THP-1 cells were incubated with 20 ng/mL PMA and 25 ng/mL IL-4 (BioLegend, San Diego, CA, USA) for 48 hours to induce M2-like macrophages. M0 and M2 THP-1-derived macrophages were incubated for 48 hours under standard culture conditions with diluted conditioned medium collected from PDT-treated cancer cells. The conditioned medium was mixed with fresh medium in a 1:1 volume ratio. After incubation with a conditioned medium, cells were collected in Trizol (Thermo Fisher Scientific, USA) for RNA extraction and gene expression study. The experimental design is summarized in Figure 1.

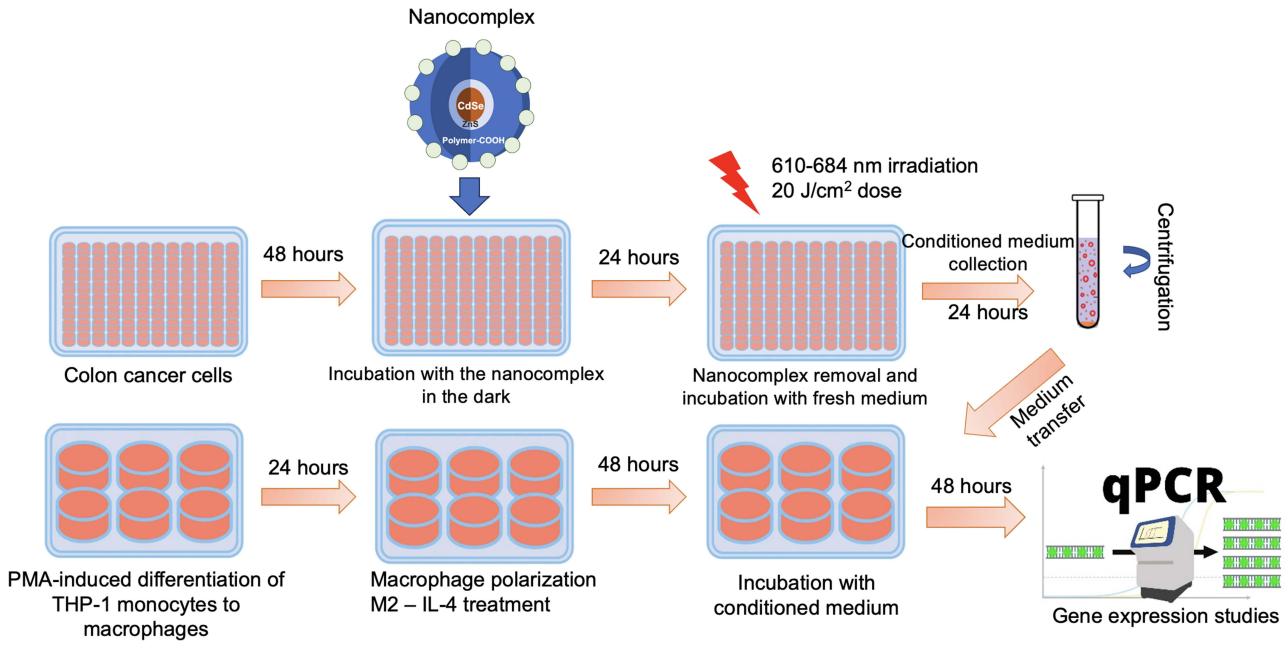

Figure 1 Preparation of conditioned medium from PDT-treated CRC cells and its application to macrophages. CRC cells were treated with the QDs-Ce6 complex, irradiated with a xenon lamp, and the conditioned medium was collected post-treatment. THP-1 cells were differentiated into M0 macrophages using PMA and further polarized into M2 macrophages with IL-4. M0 and M2 macrophages were then incubated with the conditioned medium for subsequent gene expression studies.

RNA Extraction and Gene Expression Analysis

RNA was isolated from THP-1 cells using the RNeasy Mini Kit (Qiagen, Venlo, The Netherlands) according to the manufacturer's protocol. After isolation, the quality and quantity of the RNA were assessed using a spectrophotometer (NanoDrop2000, Thermo Fisher Scientific, USA). To obtain cDNA, 500 ng of RNA from each sample was subjected to reverse transcription using Maxima First Strand cDNA Synthesis Kit (Thermo Fisher Scientific, USA) as described in accompanying instructions.

Quantitative PCR reactions were performed in 96-well plates using the Azure Cielo 3 Real Time qPCR System thermocycler (Azure Biosystems, Dublin, CA, USA). The reaction volume of 10 µL contained 2.5 µL of the 1:10 diluted cDNA reaction product, 2.5 µL of the 0.8 µM primer mix (sequences in Supplementary Table 1) (0.2 µM concentration in the final mix), and 5 µL of the Maxima SYBR Green qPCR Master Mix 2X (Thermo Fisher Scientific, USA). The qPCR conditions included initial denaturation for 5 minutes at 95 °C, then 40 cycles of denaturation for 10 seconds at 95 °C and primer attachment/polymerization for 30 seconds at 60 °C. The gene *RPL13A* was selected as a normalizing gene to evaluate the expression level of the studied genes. Three replicates were performed for each sample to ensure the reliability of the results. Gene expression analysis was performed using the $2^{-\Delta\Delta CT}$ method.

Statistical Analysis

Data were analyzed using GraphPad Prism (La Jolla, CA, USA) statistical software, averaging three independent measurements. Heatmaps of the log2 transformed gene expression profiles were generated using Morpheus tool of Broad Institute (Cambridge, MA, USA). Student's *t*-test was used to compare means. Statistically significant results are encoded in charts as *p<0.05, **p<0.01, ***p<0.0001, ***p<0.00001.

Results

Heterogeneity of CRC Cell Lines

To comprehensively understand how colorectal cancer responds to treatment, we characterized four distinct CRC lines: LS1034, SW620, HCT116, and DLD1. This array of cell lines was chosen to represent the extensive heterogeneity of

CRC, confirmed by many in vitro studies and clinical practice.[25,26] Characterization focused on evaluating the aggressiveness of CRC cell lines, including stemness properties, molecular features, and migration capacities.

Out of our selected cell lines, HCT116 and DLD1 cell lines formed large loose colonies with an undefined branched structure (Figure 2A). On the contrary, during the same 7-day period, SW620 and LS1034 cell lines developed tiny

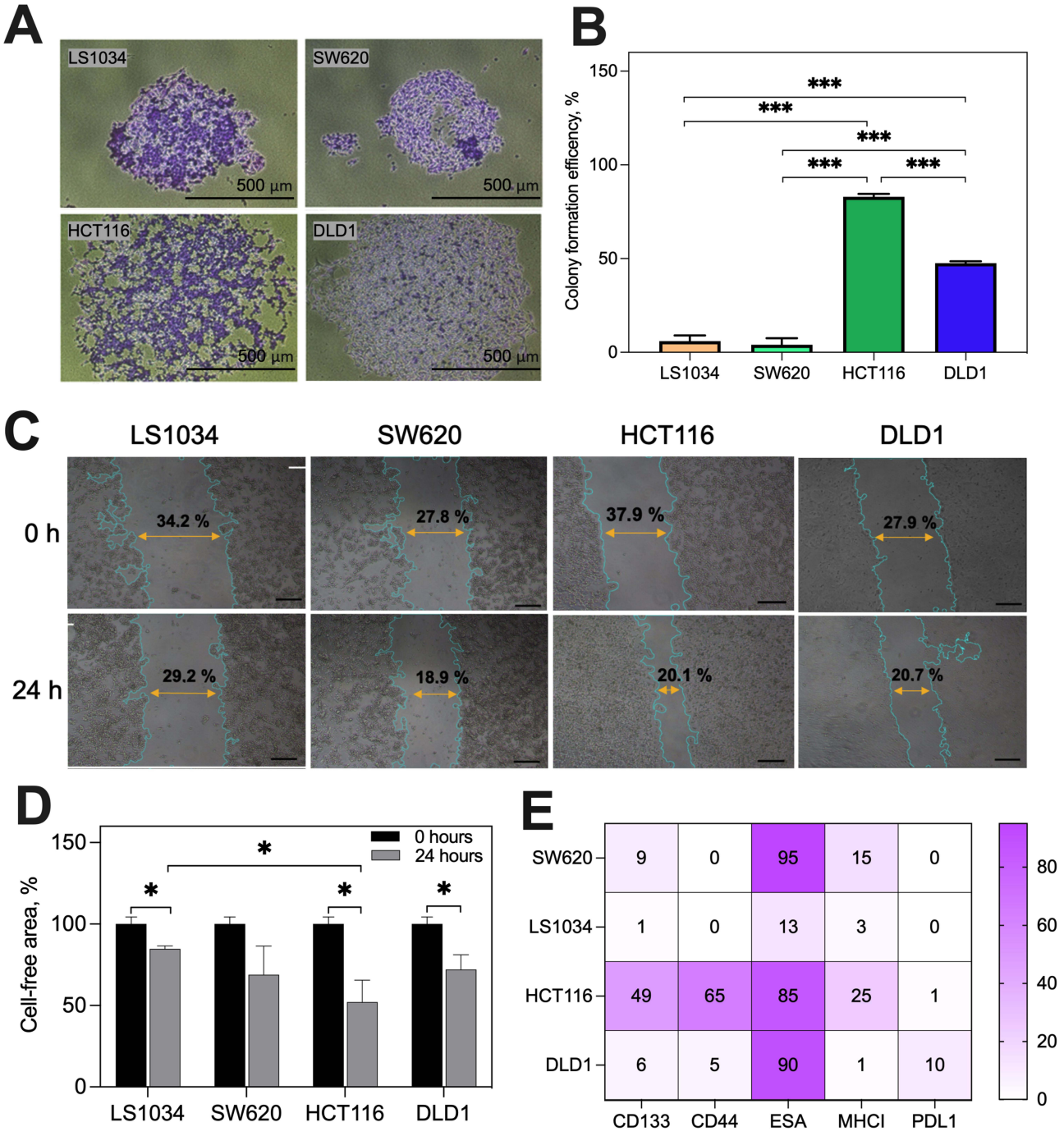

Figure 2 Characterization of four different colon cancer cell lines: SW620, LS1034, DLD1 and HCT116. Representative microscope images of the colonies in colon cancer cells. The scale bar in all pictures corresponds to 500 µm (**A**). The colony formation efficiency of colon cancer cells (**B**). Colony formation assays were performed on four cell lines. The number of colonies was calculated by analyzing the images using the ImageJ software. Representative microscope images of the wound assay to assess the migration rate of colon cancer cells (**C**). The images were taken at the initial time point (0 hour) and 24 hours later. The scale bar in all pictures corresponds to 500 µm. Changes in wound area after 24 hours were evaluated by measuring the cell-free area and expressing it as a percentage of the initial time point (0 hours) (**D**). Wound area changes after 24 hours were calculated assuming that wound area at the initial time point (0 hour) is 100%. The expression profile of surface markers associated with stemness and immunomodulation in colon cancer cell lines was investigated by flow cytometry method and represented by heatmap (**E**). Statistical significance is denoted by an asterisk (*) where $p < 0.05$*, $p < 0.001$***.

colonies (< 50 cells) with defined structure. The calculated CFE showed that HCT116 and DLD1 cell lines are significantly more clonogenic (CFE 82% and 46%, respectively) in comparison to the SW620 and LS1034 cell lines (CFE 4% and 6%, respectively) (Figure 2B). Colony formation test assesses cell proliferation and clonogenic ability, reflecting the potential of a single cell to regenerate the cancer cell population within a tumor. The results suggest that the HCT116 and DLD1 lines may exhibit more substantial stemness characteristics than the SW620 and LS1034 lines.

Cell migration is one of the hallmarks of tumor development. Figure 2C represents the visual results of the wound healing assay, which is considered a standard test for migration assessment. Changes in the wound area of CRC cells were observed from the moment of wound formation (0 hours) and after 24 hours and quantified using ImageJ software. Spontaneous cell migration occurred in all CRC cell lines (Figure 2D). HCT116 cells showed the highest migratory potential, reducing the wound area by 48%. Migration was also observed in the DLD1 (wound reduction by 28%) and SW620 (wound reduction by 31%). LS1034 cell line displayed limited migration: after 24 hours, the wound area decreased by 15%. The different migratory potential indicates the variable stemness and aggressiveness properties among the selected CRC cell lines.

For molecular characterization, the expression of stemness- and immune evasion-related surface markers was evaluated. HCT116 cell line exhibited higher stemness- and invasion-associated markers CD133 and CD44 expression levels than other cells (Figure 2E). The epithelial cell adhesion marker ESA was expressed in SW620, HCT116, and DLD1 cell lines. LS1034 and DLD1 expressed low levels of MHC I, highlighting a potential immune evasion mechanism through decreased recognition by the host immune system. Moreover, DLD1 showed the highest immune checkpoint molecule PD-L1 expression across all cell lines, likely related to the creation of immunosuppressive TME.

Together, the detailed profile of CRC cell lines, reflected in colony formation, wound healing, stemness and immunomodulatory phenotype, sets the stage for further exploration of the QDs-Ce6 nanocomplex's uptake and PDT efficacy across different cell lines.

Theranostic Potential of QDs-Ce6 Nanocomplex

To create a QDs-Ce6 nanocomplex, we mixed QDs and Ce6 in a 1:100 molar ratio. QDs are made of CdSe/ZnS core/shell with a polymer coating with carboxyl surface groups. Ce6 is an amphiphilic molecule and tends to interact with the amphiphilic polymer of QDs surface,[27] due to hydrophobic interaction between Ce6 molecule and a polymer.

Figure 3A depicts single photon absorption (SPA) and PL spectra of QDs and Ce6 solutions in RPMI-1640 medium. The absorbance of QDs decreases from the UV to the red spectral region. The PL band of QDs has a symmetrical and narrow peak at 625 nm. The absorption spectrum of Ce6 has four bands, but the most intense are the Soret band at 405 nm and the Q band at 650 nm. The fluorescence spectrum of Ce6 has a maximum of 660 nm. If QDs-Ce6 nanocomplex was to be utilized as a "switch on" and "switch off" platform, the excitation of QDs-Ce6 by 980 nm would result in PL of QDs only (diagnostic imaging). In comparison, excitation of 650 nm would result in excitation of Ce6 only (photodynamic therapy).

Singlet oxygen and ROS are the main inducers of damage to cellular components such as proteins, lipids, DNA, and carbohydrates, leading to cell death. To assess the ability of QDs-Ce6 to generate singlet oxygen, we used the SOSG sensor, which is highly selective for singlet oxygen.[24] In Figure 3B, the calculated SOSG fluorescence intensity (Δ_{SOSG}) was depicted as a function of irradiation dose (J/cm^2). As expected, upon irradiation of the xenon lamp (650/70 nm bandpass filter), the Δ_{SOSG} increased in both the QDs-Ce6 and Ce6 samples. Surprisingly, the Δ_{SOSG} was 2.2-fold higher in the QDs-Ce6 sample, although the concentration of Ce6 was the same in both samples. QDs without Ce6 did not cause a change in the ΔI_{SOSG}, indicating that singlet oxygen was not produced.

TPA is a non-linear process that requires high photon intensity per area.[28] In Figure 3C, the QDs-Ce6 nanocomplex was suspended in RPMI-1640 medium and excited by continuous wave 980 nm laser (TPA conditions) with varying excitation powers. As the excitation power increases, PL intensity also increases. Moreover, the PL intensity of QDs is linearly dependent on the power of the laser once depicted at the logarithmic scale (Figure 3C, insert). Therefore, the multiphoton excitation process is present with a k constant of 2.1171, indicating the absorption of 2 photons. Laser excitation by 980 nm causes minimal fluorescence signal of Ce6, indicating that QDs-Ce6 can function as a versatile

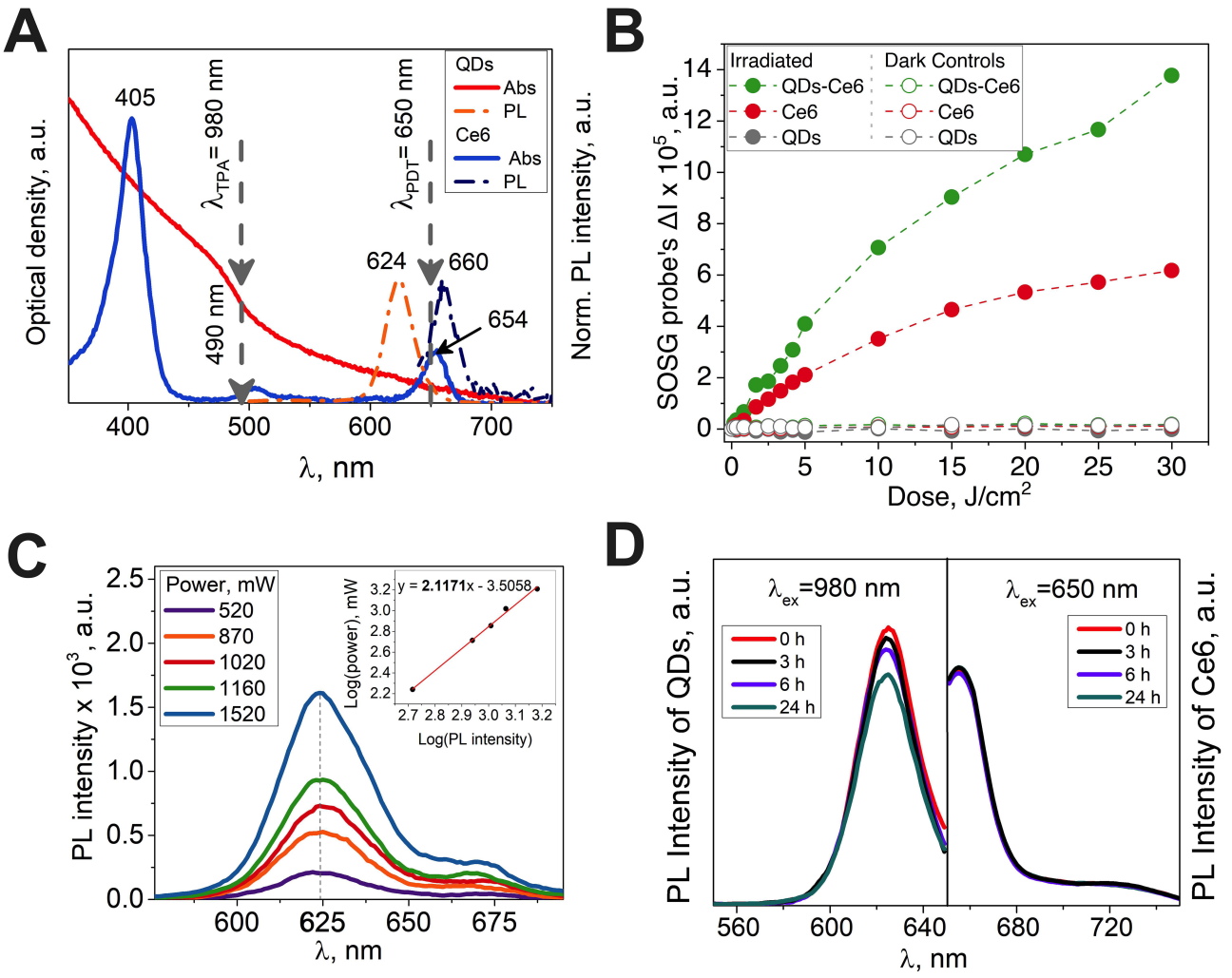

Figure 3 Characterization of the QDs-Ce6 nanocomplex. Normalized absorption and photoluminescence (PL) spectra of QDs and Ce6 solutions in RPMI-1640 medium (without phenol red) (**A**). The arrow at 490 nm indicates a wavelength used for SPA and corresponding TPA at 980 nm excitation of the samples. The line at 650 nm indicates the absorption band of Ce6 used for PDT therapy. (**B**) – Singlet oxygen generation capacity of QDs-Ce6 detected by SOSG probe. Samples were irradiated with xenon light (650/70 nm bandpass filter). (**C**) - Photoluminescence of QDs-Ce6 nanocomplex in RPMI-1640 medium after excitation by 980 nm laser with varying power (from 520 mW to 1520 mW). Insert of (**C**) shows derived data and mathematical approximation (straight line function) for assessment of multiphoton process. The stability of the nanocomplex was assessed by measuring PL spectra after different time intervals of incubation: 0, 3, 6, and 24 hours in RPMI-1640 medium (**D**). Two excitation wavelengths were used: λ_{ex} = 980 nm and λ_{ex} = 650 nm.

theranostic platform that can be selectively switched between diagnostic and therapeutic modes depending on the excitation wavelength.

Since nanocomplex incubation with cells lasted 24 hours, the stability of QDs-Ce6 nanocomplex was also followed for 24 hours. Figure 3D shows the time-dependent colloidal stability of the nanocomplex under excitation of 980 nm and 650 nm. After 3 hours and 6 hours, almost no change was observed in the PL intensity of Ce6, while a slight decrease in the PL signal of QDs was observed (<8%). After 24 hours, PL signal of QDs continued to decrease, and reached 84% of its initial intensity value. Ce6 signal did not change throughout the whole experiment.

To sum up, we proved the capability of QDs-Ce6 to respond to TPA excitation by a 980 nm laser (imaging) and SPA excitation by 650 nm (photodynamic therapy). Singlet oxygen generation was achieved upon photodynamic therapy excitation (650/70 nm bandpass filter). The stability of the nanocomplex in the biological medium was appropriate; therefore, we continued the experiments with CRC cells.

Uptake and Localization of QDs-Ce6 Nanocomplex in Cancer Cells

We next evaluated the cellular uptake and distribution of the QDs-Ce6 nanocomplex in each CRC cell line. The transmission microscopy images revealed that all cell lines used in this study were similar in size, but different in morphology. LS1034 and HCT116 form clusters, while SW620 and DLD1 display spread-like growing pattern (Figure 4A).

Figures 4B and C show PL signal overlay with transmission images at different magnifications. The nanocomplex is observed to accumulate across all types of cells in vesicle-like structures inside the cytoplasm but not in the nuclei. For a more precise analysis, spectral data of the nanocomplex accumulated inside the cells was collected from each region of interest (Figures 4D and 3E). The excitation of the 488 nm laser resulted in PL spectra of two peaks: 626 nm, which can be attributed to QDs, and 673 nm, which can be attributed to Ce6. It is important to mention that 488 nm excitation is very close to 490 nm (TPA=980 nm) excitation used in spectroscopic characterization of nanocomplex in solutions (Figure 3C). The obtained PL spectra from different regions of interest in cells (Figure 4E) are comparable to the PL spectrum of QDs-Ce6 obtained in RPMI solutions (Figure 3C).

These observations reveal that the QDs-Ce6 nanocomplex is engulfed within 24 hours and localizes within cytoplasmic structures regardless of the heterogeneity of CRC cell lines.

Accumulation Dynamics and Biocompatibility of QDs-Ce6 Nanocomplex

To determine the quantitative accumulation dynamics of nanocomplex in cells, time points of 1, 3, 6, and 24 hours were selected to evaluate the uptake of QDs-Ce6 nanocomplex. The increase in fluorescence signal reflects the relative amount of accumulated nanocomplex. 1 hour of incubation resulted in a detectable fluorescence signal of QDs-Ce6 in all CRC cell lines (Figure 5A). Extended incubation time led to an even higher increase in the fluorescence signals, indicating progressive accumulation of the nanocomplex. After 24 hours, the accumulation of nanocomplex was similar across all cell lines, as indicated by the fluorescence signals (Figure 5B). A slightly higher signal can be registered in the DLD1 cell line. However, no statistical significance was proven ($p=0.309$).

The CCK-8 assay, measuring cell viability through metabolic activity, was used to evaluate the dark toxicity and biocompatibility of nanocomplex in the CRC cells (Figure 5C). Cells were evaluated after 24 hours of incubation with QDs-Ce6 nanocomplex at concentrations of 5 nM, 16 nM and 25 nM (QDs:Ce6 ratio 1:100). The nanocomplex was biocompatible, except for 25 nM concentration in LS1034 cell line, where the viability was less than 70%.

Although CRC cells have different properties, their ability to accumulate the nanocomplex remains consistent. The biocompatibility of the QDs-Ce6 nanocomplex is consistent at appropriate concentrations, supporting its further use in this study. The concentration of 16 nM was selected to balance effective uptake and minimal cytotoxicity.

Photodynamic Efficacy of Nanocomplex Across Different Cancer Cell Lines

Before evaluating the therapeutic potential of the QDs-Ce6 nanocomplex, we decided to test the sensitivity of CRC cell lines to standard chemotherapy drug 5-FU (Figure 6A). After 48 hours of 5-FU treatment, the viability measurement highlighted DLD1 (IC50=2 μM) as the least sensitive cell line, compared to other cell lines, in which IC50 was almost 10 times lower (0.02–0.03 μM) (Table 1). Although HCT116 cells possessed high expression of stemness markers, high CFE, and migratory capacity (Figure 2), they were ten times more sensitive to 5-FU than DLD1 (Figure 6B). This variability in 5-FU sensitivity highlights the therapeutic challenges associated with pharmacological CRC treatment.

Since LS1034 and DLD1 cell lines showed the most pronounced differences in molecular characteristics (Figure 2A–E) and a ten-fold difference in sensitivity to 5-FU (Figure 6B), they were selected to assess the effects of nanocomplex-assisted PDT. Cells were incubated with the nanocomplex for 24 hours and were irradiated with a xenon lamp at doses of 10, 20, and 30 J/cm^2. Cytotoxicity was evaluated using the CCK-8 assay. The results suggest that LS1034 and DLD1 cell lines responded similarly to nanocomplex-induced PDT (Figure 6C). Upon increasing the doses of light irradiation, the viability of CRC cells has decreased. Despite varying subtypes and chemotherapy-resistant characteristics of LS1034 and DLD1, the efficacy of nanocomplex-assisted PDT is equally effective among these cells.

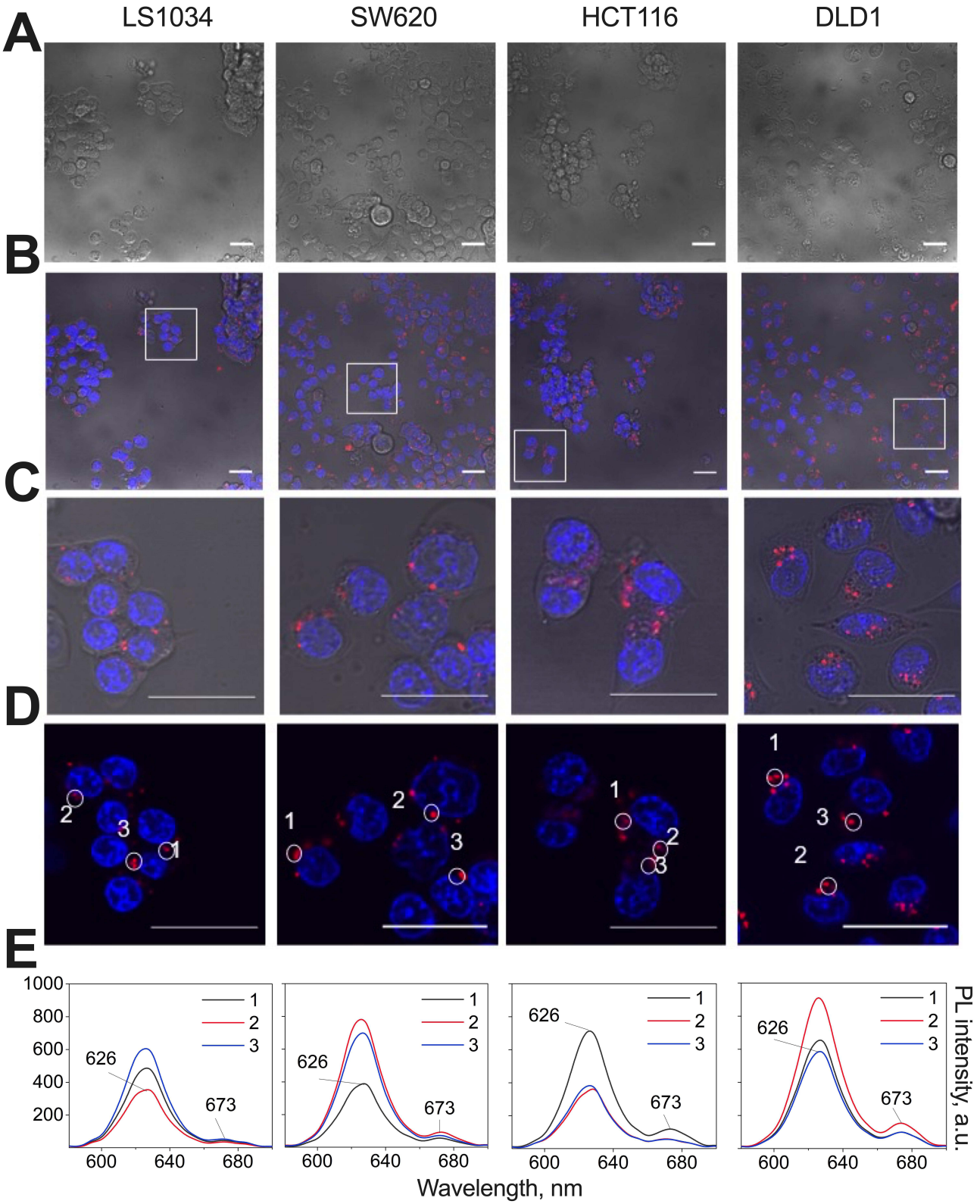

Figure 4 Confocal microscopy images of the QDs-Ce6 complex accumulation in colon cancer cell lines: LS1034, SW620, HCT116 and DLD1. (**A**) row represents transmission images (TI) of the corresponding CRC cells; (**B**) row represents laser scanning confocal images combined with TI: blue indicates nuclei, stained by Hoechst (λ_{ex} = 404 nm) and red indicates PL of QDs-Ce6 nanocomplex, (λ_{ex} = 488 nm); (**C**) row shows the zoomed view of the cells from images in (**B**); (**D**) row represents areas where spectra of the QDs-Ce6 was registered and depicted in (**E**) row. Numbers 1, 2, 3 in (**D** and **E**) represent distinct intracellular regions of interest selected within single cells for QDs-Ce6 photoluminescence intensity measurements. Cell images are shown in a wide-field (**A** and **B**) and 4.4x zoomed (**C** and **D**) view. Scale bars in all images are 25 μm.

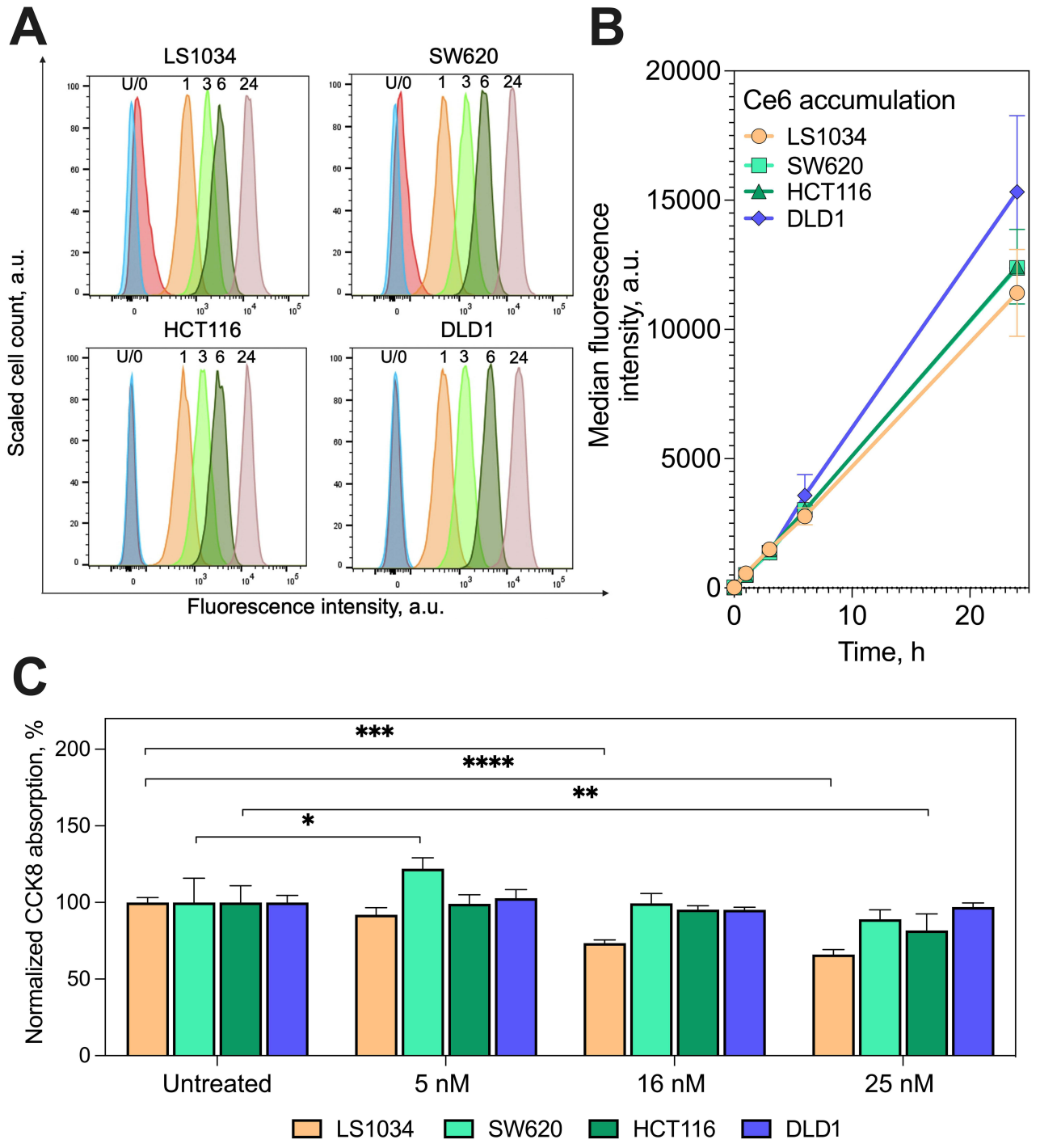

Figure 5 Accumulation dynamics and biocompatibility of the QDs-Ce6 complex in colon cancer cells. QDs-Ce6 complex accumulation in colon cancer cells after 1, 3, 6, and 24 hours incubation (**A**). Fluorescence intensity of QDs-Ce6 in histograms on the X-axis, Y – number of cells. Graphical representation of the accumulation dynamics of the QDs-Ce6 complex in cancer cells by FIM (median fluorescence intensity) (**B**). Colon cancer cells were incubated in the dark with different concentrations of QDs-Ce6 nanocomplex (5 nM, 16 nM, 25 nM) for 24 hours and evaluated with CCK-8 cytotoxicity assay (**C**). Statistically significant differences compared to the control were indicated by an asterisk (*) (*p<0.05; **p<0.01 ***p<0.001; ****p<0.00001). U/0 - unlabeled.

Overall, these results demonstrate that the QDs-Ce6 nanocomplex offers a consistent photodynamic effect despite diversity in CRC cell lines linked to inherent aggressiveness and provides an effective alternative or complementary approach to 5-FU, especially for cells that are less responsive to chemotherapy.

https://doi.org/10.2147/IJN.S518050

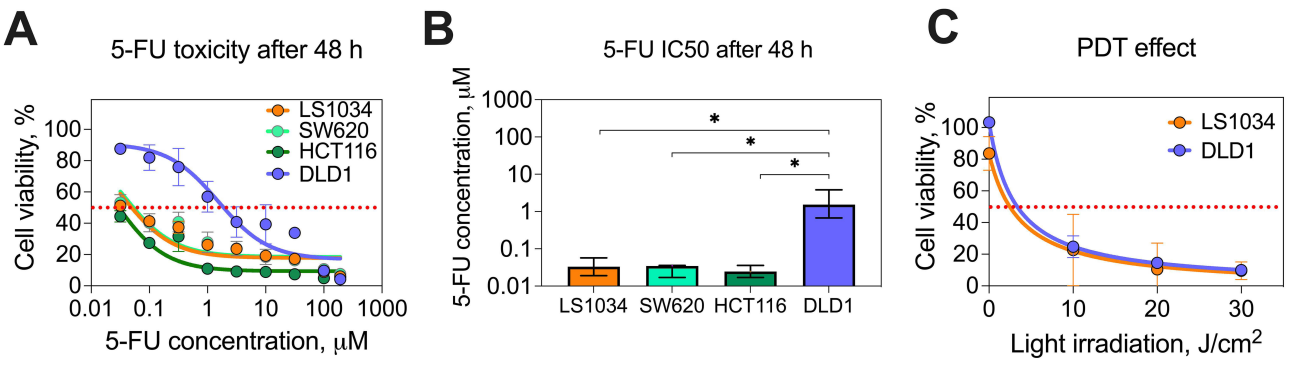

Figure 6 Treatment efficacy of 5-FU and QDs-Ce6 nanocomplex. Cytotoxicity experiments of 5-FU were performed to compare the sensitivity of SW620, HCT116, DLD1 and LS1034 cell lines to chemotherapy (**A**) and to estimate the inhibition values after 48 hours of treatment (**B**). Efficacy of nanocomplex-induced PDT was investigated by applying 10 J/cm², 20 J/cm² and 30 J/cm² light doses in DLD1 and LS1034 cell lines (**C**). The concentration of QDs-Ce6 was 16 nM. Statistically significant differences compared to the control were indicated by an asterisk (*) (*p<0.05).

Immunomodulatory Effect of Nanocomplex-Induced PDT on Tumor-Associated Macrophages

Beyond the direct QDs-Ce6 nanocomplex cytotoxic effects on CRC cells, we further explored the potential of nanocomplex-induced PDT to modulate the immune TME, specifically by assessing its influence on macrophage phenotypes through conditioned media from treated CRC cells. DLD1 and LS1034 cell lines, selected for their distinct levels of aggressiveness and drug sensitivity, were utilized in these experiments. We adopted THP-1-derived M2 (pro-tumoral polarized) and M0 (non-polarized) macrophage models to represent better typical resident TAMs and newly recruited TAM of monocytic origin, respectively. M2-polarized or M0 non-polarized macrophages were incubated for 48 hours in a conditioned medium collected from PDT-treated cancer cells, mixed in a 1:1 ratio with fresh complemented RPMI-1640 medium. The changes in gene expression upon incubation to conditioned medium were analyzed to evaluate macrophage phenotype shifts towards either pro-tumoral or anti-tumoral state.

The data suggest that conditioned medium from DLD1 and LS1034 cells, treated with nanocomplex alone or with nanocomplex-assisted PDT, induced different phenotypical changes on M2 and M0 macrophages, with notable variations between the effects of each cell line (Figure 7). In the M2 macrophages (resident TAM model), conditioned medium from LS1034 cells did not induce any significant changes in marker expression, with similar profiles observed for both nanocomplex alone and nanocomplex+PDT treatments. There was a slight, non-significant trend towards increased

Table 1 Inhibitory Concentration (IC50) Values with 95% Confidence Intervals (CI) of 5-Fluorouracil and QDs-Ce6 Nanocomplex-Induced Photodynamic Therapy in Different Colon Cancer Cell Lines

5-fluorouracil		
Cell line	**IC50 (μM)**	**95% CI (μM)**
DLD1	1.53	0.67–3.84
LS1034	0.03	0.02–0.06
HCT116	0.02	0.02–0.04
SW620	0.03	0.02–0.06
QDs-Ce6 nanocomplex-induced photodynamic therapy		
Cell line	**IC50 (J/cm²)**	**95% CI (J/cm²)**
DLD1	3.11	1.80–4.70
LS1034	3.75	0.00–15.66

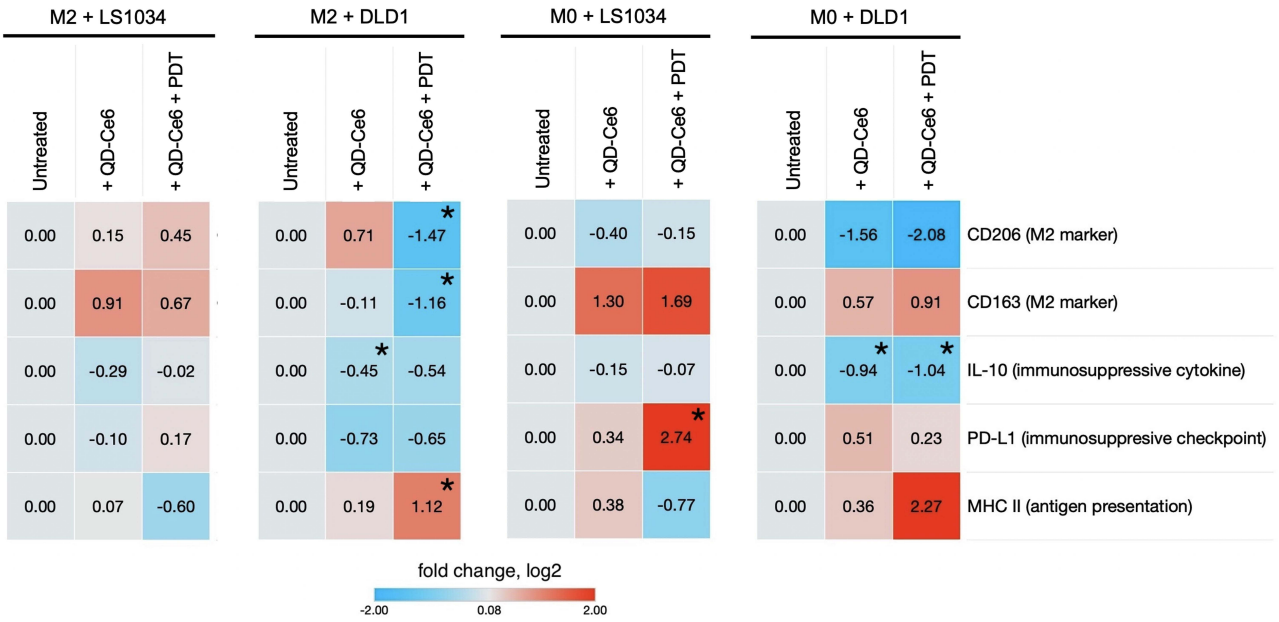

Figure 7 Macrophage phenotype changes after exposure to a conditioned medium from CRC cells treated with nanocomplex-induced PDT. M2-polarized or M0 non-polarized THP-1-derived macrophages were exposed for 48 hours to a conditioned medium collected from PDT-treated LS1034 (left panel) or DLD1 (right panel) cell lines in a 1:1 ratio with fresh complemented RPMI medium. The log2-transformed relative gene expression levels are depicted in the heatmap with different color intensities. Each square represents the mean relative expression value from two independent experiments with two technical repeats normalized to the expression levels in macrophages exposed to medium from untreated CRC cells. Significant changes ($p < 0.05$) are marked with an asterisk (*). LS - LS1034 cell line, DLD - DLD1 cell line.

expression of CD163 in both conditions. In contrast, conditioned medium from DLD1 cells had a more pronounced effect, inducing a modest but significant reduction in IL-10 following exposure to the nanocomplex alone. Upon PDT treatment, DLD1-conditioned medium led to a notable, biologically relevant decrease (over twofold) in the M2 markers CD206 and CD163, accompanied by an increase in the antigen presentation molecule MHC II, suggesting a shift from a pro-tumoral to a more anti-tumoral phenotype in resident TAM model.

In the M0 macrophages (recruited TAM model), LS1034-conditioned medium appeared more effective than in M2 model, suggesting that unpolarized macrophages (M0) may be more susceptible to phenotype shifts than pre-polarized M2 macrophages. Both nanocomplex alone and nanocomplex+PDT treatments notably increased the M2 marker CD163, and the nanocomplex+PDT condition significantly upregulated the immunosuppressive checkpoint molecule PD-L1. On the other hand, conditioned medium from DLD1 cells treated with the nanocomplex alone already showed a reduction in the M2 marker CD206 and a significant decrease in IL-10 in M0 macrophages. Following PDT, this phenotype persisted, along with further upregulation of MHC II, similarly as in the M2 model.

These findings reveal that QDs-Ce6 nanocomplex-induced PDT directly targets CRC cells and reprograms macrophages within the tumor microenvironment. Conditioned medium from DLD1 cells, a chemotherapy-resistant line with high stemness and immune evasion properties, proved especially effective in shifting macrophage phenotypes: it significantly reduced pro-tumoral markers and increased MHC II expression in both M0 and M2 macrophages, indicating a reprogramming towards an anti-tumoral state. In contrast, LS1034-conditioned medium primarily affected M0 macrophages, with limited impact on M2 macrophages. These results highlight the potential of the QDs-Ce6 nanocomplex in modulating TAMs, particularly in aggressive and resistant CRC types like DLD1, to enhance immune responses.

Discussion

This study highlights the potential of the QDs-Ce6 nanocomplex as a tool for both direct cancer cell eradication and modulation of the non-cancer cells in TME. The demonstrated cytotoxic effect of QDs-Ce6 nanocomplex-induced PDT on CRC cell lines, including the chemotherapy-resistant DLD1, was further investigated through conditioned medium experiments in TAM models, revealing that the nanocomplex treatment also influences macrophage phenotypes. These

findings suggest the potential translational relevance of our study, simulating a scenario where cancer cells internalize nanoparticles, undergo PDT, and subsequently upon cell death release factors that modulate TAMs, the most abundant cells in TME.

Numerous studies have proven the high quantum yield and photostable luminescence of QDs, which can be applied for long-term cell tracking or labeling.[29,30] Ce6 is a second-generation photosensitizer with a very efficient singlet oxygen generation.[31,32] The complex of QDs and Ce6 has become a convenient nanomedicine tool. It can be easily assembled and broadly applied in biomedical studies to explore the theranostic features of nanoparticle-photosensitizer constructs.[9,10,27] We aimed to use this well-established nanocomplex and explore its immunomodulatory potential together with eradication of aggressive types of cancer cells. When QDs are assembled into a nanocomplex with Ce6, they efficiently generate singlet oxygen, a form of ROS.[33,34] In our study, we compared the singlet oxygen generation capacity of Ce6 and QDs-Ce6, revealing QDs-Ce6 superiority. Moreover, we used a continuous-wave 980 nm laser source to demonstrate the two-photon absorption (TPA) effect in the QDs-Ce6 nanocomplex. In a typical single-photon excitation, the QD absorbs a photon whose energy matches the energy gap between its ground state and an excited electronic state.[35] In TPA, the QD absorbs two photons simultaneously instead of a single photon with enough energy to bridge the gap.[36] In our study, we chose to use 980 nm laser, because it is often used in biological imaging, as it allows for deeper tissue penetration with less photodamage due to the use of longer-wavelength excitation.[36]

The idea of theranostic nanoplatforms with decoupled diagnostics and therapy has been proposed in our previous article.[3] Other studies have also explored the development of theranostic nanoparticles by combining near infrared fluorophores (for diagnostics and treatment monitoring) with therapeutic drugs.[37,38] In this study, we used 980 nm (infrared) laser and xenon lamp with bandpass filter 650/70 nm (red) to activate the nanocomplex in the tissue transparency window.[39] 980 nm laser activates the photoluminescence of QDs, while only a minimal portion of Ce6 is excited (absorption of Ce6 is minimal at 980/2=490 nm). The excitation of QDs via TPA has been documented before,[40] but in the current study, for the first time, a continuous wave 980 nm laser induced a non-linear optical process in QDs. Moreover, PL signal of QDs increased when laser power was elevated and the k constant of linear function equaled to ~2, indicating a two-photon process. Using a femtosecond pulsed laser with much higher power density could result in three- or even four-photon absorption.[41] Colloidal stability measurements of the nanocomplex in RPMI-1640 medium showed that nanocomplex is stable enough for 24 hours. Other studies also documented that the self-assembled nanocomplex retains its stability for 24 hours, but longer incubation of QDs-Ce6 in cell medium might result in a loss of PL signal.[10]

To fully evaluate the therapeutic and diagnostic potential of QDs-Ce6 nanocomplex, we explored its effects on a diverse panel of CRC cell lines. This approach allowed us to understand how CRC heterogeneity influences the nanocomplex's efficacy and offers insights into its application across various tumor subtypes. Consensus molecular subtypes (CMS) classification of CRC tumors defines four categories: immune-mediated CMS1 subtype, canonical CMS2 subtype, metabolic CMS3 subtype, and mesenchymal CMS4 subtype.[26] This classification is based on differential transcriptomic profiling and refers to specific tumor biology and clinicopathological features. In our study, we selected CRC cell lines, earlier stratified according to the CMS subtypes: DLD1 as CMS1, LS1034 as CMS2, HCT116 and SW620 as CMS4.[25]

Building on the already reported CMS classification, we also observed differences in aggressiveness-related features in selected CRC cell lines, including stemness properties (clonogenicity and migration), specific surface phenotype, and drug sensitivity. HCT116 and DLD1 cell lines had higher colony formation efficiency, suggesting stronger proliferative potential compared to the SW620 and LS1034 lines. Cell migration, a hallmark of tumor progression and metastasis, is stimulated by growth factors and chemokines that activate complex signaling pathways involved in cell motility.[42] Our results show that cell migration occurred in all CRC lines upon wound formation, but their migratory potential differed. Migration in HCT116 and SW620 cell lines can be determined by their CMS4 mesenchymal molecular subtype and high expression of stemness markers - CD133 and CD44.[43,44] This assumption is supported by the surface phenotype findings, as HCT116 cells showed high expression of CD44 and CD133, and the SW620 line showed expression of CD133. Migration of DLD1 cells is associated with an increase in SNAIL1, which causes changes in the morphology of these cells and reduces the expression of the epithelial phenotype marker E-cadherin, leading to increased motility and invasiveness of these cells.[45] Furthermore, our surface marker expression studies showed that the SW620, HCT116,

and DLD1 cell lines highly express the ESA marker. Overexpression of ESA enhances the properties of cellular adhesion and contributes to increased cell migration and closely correlates with tumor progression.[46] The LS1034 cell line is less aggressive than other CRC lines due to its lower proliferation and invasion. This cell line typically exhibits reduced metastatic potential and lower expression of markers associated with cancer stemness and epithelial-mesenchymal transition, both critical in promoting tumor aggressiveness and spread.[47]

The phenotypic and functional diversity among CRC cell lines provided a basis for evaluating the QDs-Ce6 nanocomplex's efficacy across different cells. Before performing PDT effect by 650 nm light irradiation, we evaluated the dark toxicity of QDs-Ce6 nanocomplex and explored the accumulation dynamics. Currently, there is no data in the literature on the biocompatibility of the QDs-Ce6 nanocomplex with CRC cell lines. Our results showed that at concentrations of 5 nM and 16 nM, the viability of all cell lines was greater than 73%, indicating good biocompatibility in the dark. According to ISO 10993–5 standards,[48] nanoparticles are considered non-toxic when cell viability exceeds 70% after treatment. Based on the obtained results and literature,[23] we conducted accumulation studies of the nanocomplex at a concentration of 16 nM. Our results showed that the QDs-Ce6 nanocomplex can accumulate in all CRC cell lines, regardless of their molecular characteristics, and the amount of the QDs-Ce6 nanocomplex in the cells depends on the incubation time. Microscopy images revealed a vesicular uptake pattern across all CRC cell lines and were in good agreement with our previous studies: QDs-Ce6 accumulate in human skin mesenchymal stem cells MSCs)[10] cancer cell lines such as MiaPaCa2 and[9] MDA-MB-231.[10] Spectral imaging of CRC cells proved the presence of typical QDs-Ce6 spectral bands inside vesicular structures.

In assessing the response of CRC cells to the chemotherapeutic drug 5-FU, the DLD1 cell line appeared to be least sensitive across all tested cell line (IC50=2 μM in DLD1 vs 0.03 μM in others). Since the aggressiveness of cancer cells has been related to the development of drug resistance,[49] the DLD1 cell line emerged as the most aggressive and able to withstand 5-FU treatment. Resistance to 5-FU is linked to high stemness properties in cancer cells.[50] The stronger stemness characteristics (clonogenicity, migration, surface phenotype) observed in DLD1 cell line (compared to LS1034) likely contribute to lower sensitivity to 5-FU.

The comparison of nanocomplex-induced PDT and 5-FU on two CRC cell lines with varying levels of aggressiveness (LS1034 and DLD1) revealed the consistent, dose-dependent cytotoxic effects of QDs-Ce6-mediated PDT, independent of the intrinsic cell line molecular properties. This consistency contrasts with the variable responses observed in 5-FU chemotherapy among different molecular subtypes of cancer cells[51] and highlights the PDT as an effective approach for cells that are less responsive to chemotherapy.

As a final step of our study, we evaluated the effect of PDT-assisted treatment for resident and recruited TAMs. Various therapies targeting cancer cells also affect other cells in TME.[52] Moreover, nanoparticle-based chemodynamic therapy has been shown to trigger immunogenic death of cancer cells, thereby reversing the immunosuppressive TME and enhancing antitumor immune responses.[53] TAMs, an abundant and plastic population of tumor-infiltrating cells, are a potential target for remodeling the immunosuppressive tumor microenvironment.[54] We investigated macrophage phenotype changes after exposure to conditioned medium from CRC cells treated with nanocomplex-induced PDT. Despite the similar quantitative response of different CRC cells, LS1034 and DLD1, to nanocomplex-induced PDT, we observed that their conditioned medium exerted distinct effects on TAMs. The resident and recruited TAMs were represented by induced M2 and M0 states of THP-1 monocytes. Furthermore, our results suggest that the nanocomplex has the potential to modulate the function of naïve recruited M0 macrophages by influencing their polarization and subsequent role in immune responses. The results showed that the conditioned medium of LS1034 cells after nanocomplex-induced PDT did not induce significant transcriptional changes in M2 macrophages. On the contrary, the conditioned medium of PDT-treated DLD1 cell line significantly decreased the gene expression of the M2 markers CD206 and CD163 and significantly increased the gene expression of the antigen presentation molecule MHC II in M2 macrophages. Similar effect was also observed in unpolarized M0 macrophages - the conditioned medium of PDT-treated DLD1 significantly decreased the expression of major immunosuppression orchestrator – IL-10. These results support the assumption of the anti-tumor immunomodulatory effect of the theranostic nanocomplex-induced PDT-treated aggressive cancer cells which can reshape TME by repolarizing macrophages from pro-tumoral to anti-tumoral state. Notably, the observed effects of DLD1 cell line align with its characteristics of immune activation and CMS1 subtype classification.

So far, several theranostic nanodrugs designed to directly target macrophage were reported in the in vivo models of atherosclerotic plaque,[55–57] as macrophages play a central role in mediating inflammation at every stage of atherosclerosis. In

cancer research, although various studies have explored the impact of nanoparticle treatments on macrophage polarization,[58–61] there is still no standardized method to assess these effects. Factors such as surface functionalization, chemical composition, and size can influence macrophage response. Iron nanoparticles, for example, have been shown to strongly induce antitumoral phenotype in TAMs,[62] highlighting the potential of nanoparticle design as key factor for modulating immune responses. Theranostic nanoplatforms designed to induce PDT may enhance macrophage activation within the TME, as the photodynamically killed tumor cells could indirectly stimulate macrophages' antitumor activity.[63] As a proof of principle, intravenously injected monosaccharide-conjugated Ce6 was shown to kill cancer cells and shift TAMs into M1 upon inducing PDT in vitro and in mouse subcutaneous tumor model.[64,65] Ce6 photosensitizer coupled with small molecule as a self-assembly nanomedicine in breast cancer model also proved effective in antitumoral macrophage polarization.[66] A study using AGuIX nanoparticles with porphyrin as the photosensitizer demonstrated preferential uptake by M2 macrophages over M1. Following PDT, the secretome from treated glioblastoma cells induced a shift in THP-1-derived M2 macrophages toward an M1 phenotype.[67]

Conclusion

In the current context, our study stands out by demonstrating the theranostic functionality of QDs-Ce6 nanocomplex by using a "switch on" and "switch off" approach with two different sources of light: 980 nm for imaging and 650 nm for eradication of all types of CRC cells and reprogramming TAMs. Unlike previous studies that rely on simpler photosensitizers or specific molecular conjugates, our approach leverages a versatile theranostic nanoplatform that enables separation between imaging and PDT modes. Moreover, despite molecular and functional differences in CRC subtypes, the accumulation and PDT effect of QDs-Ce6 was comparable, contrary to chemotherapy effect by 5-FU. QDs-Ce6 proved successful in eradicating the aggressive chemotherapy-resistant DLD1, and subsequently induced antitumoral phenotype in both TAM and recruited macrophages post-PDT.

Despite emerging potential of QDs-Ce6, our study has several limitations. First, it is conducted in vitro, which may not fully capture the complex interactions of an in vivo environment and therefore calls for further validation in more physiologically relevant contexts, such as 3D cultures or animal models. Future studies should also address the in vivo biodistribution and biosafety profile of the nanocomplex to support its translational applicability. Additionally, testing the versatility of nanocomplex outside of colorectal cancer could confirm its broader applicability.

Acknowledgments

A.B., E.K., A.M., S.S. acknowledge support from the grant "Mesenchymal stem cells as vehicles for targeted delivery of theranostic nanoparticles into aggressive type of cancer cells" No. S-MIP-22-31.

Disclosure

The authors report no conflicts of interest in this work.

References

1. Correia JH, Rodrigues JA, Pimenta S, Dong T, Yang Z. Photodynamic therapy review: principles, photosensitizers, applications, and future directions. *Pharmaceutics*. 2021;13(9):1332. doi:10.3390/PHARMACEUTICS13091332
2. Fritsch C, Ruzicka T. Fluorescence diagnosis and photodynamic therapy in dermatology from experimental state to clinic standard methods. *J Environ Pathol Toxicol Oncol*. 2006;25(1–2):425–439. doi:10.1615/JENVIRONPATHOLTOXICOLONCOL.V25.I1-2.270
3. Skripka A, Karabanovas V, Jarockyte G, et al. Decoupling theranostics with rare earth doped nanoparticles. *Adv Funct Mater*. 2019;29(12):1807105. doi:10.1002/ADFM.201807105
4. Ning Y, Liu YW, Yang ZS, et al. Split and Use: structural Isomers for Diagnosis and Therapy. *J Am Chem Soc*. 2020;142(14):6761–6768. doi:10.1021/JACS.0C01155/SUPPL_FILE/JA0C01155_SI_005.CIF
5. Arranja AG, Pathak V, Lammers T, Shi Y. Tumor-targeted nanomedicines for cancer theranostics. *Pharmacol Res*. 2017;115:87–95. doi:10.1016/J.PHRS.2016.11.014
6. Valanciunaite J, Klymchenko AS, Skripka A, et al. A non-covalent complex of quantum dots and chlorin e6: efficient energy transfer and remarkable stability in living cells revealed by FLIM. *RSC Adv*. 2014;4(94):52270–52278. doi:10.1039/C4RA09998B
7. Shliakhtsin SV, Trukhachova TV, Isakau HA, Istomin YP. Pharmacokinetics and biodistribution of Photolon® (Fotolon®) in intact and tumor-bearing rats. *Photodiagnosis Photodyn Ther*. 2009;6(2):97–104. doi:10.1016/J.PDPDT.2009.04.002
8. Isakau HA, Parkhats MV, Knyukshto VN, Dzhagarov BM, Petrov EP, Petrov PT. Toward understanding the high PDT efficacy of chlorin e6–polyvinylpyrrolidone formulations: photophysical and molecular aspects of photosensitizer–polymer interaction in vitro. *J Photochem Photobiol B*. 2008;92(3):165–174. doi:10.1016/J.JPHOTOBIOL.2008.06.004

9. Steponkiene S, Valanciunaite J, Skripka A, Rotomskis R. Cellular uptake and photosensitizing properties of quantum dot-chlorin e6 complex: in vitro study. *J Biomed Nanotechnol*. 2014;10(4):679–686. doi:10.1166/JBN.2014.1738
10. Dapkute D, Pleckaitis M, Bulotiene D, Daunoravicius D, Rotomskis R, Karabanovas V. Hitchhiking nanoparticles: mesenchymal stem cell-mediated delivery of theranostic nanoparticles. *ACS Appl Mater Interfaces*. 2021;13(37):43937–43951. doi:10.1021/acsami.1c10445
11. Yu N, Huang L, Zhou Y, Xue T, Chen Z, Han G. Near-infrared-light activatable nanoparticles for deep-tissue-penetrating wireless optogenetics. *Adv Healthc Mater*. 2019;8(6). doi:10.1002/ADHM.201801132
12. Xu L, Zhang J, Yin L, Long X, Zhang W, Zhang Q. Recent progress in efficient organic two-photon dyes for fluorescence imaging and photodynamic therapy. *J Mater Chem C Mater*. 2020;8(19):6342–6349. doi:10.1039/D0TC00563K
13. Larson DR, Zipfel WR, Williams RM, et al. Water-soluble quantum dots for multiphoton fluorescence imaging in vivo. *Science*. 2003;300 (5624):1434–1436. doi:10.1126/SCIENCE.1083780
14. Sadanandam A, Lyssiotis CA, Homicsko K, et al. A colorectal cancer classification system that associates cellular phenotype and responses to therapy. *Nat Med*. 2013;19(5):619. doi:10.1038/NM.3175
15. Hrudka J, Kalinová M, Fišerová H, et al. Molecular genetic analysis of colorectal carcinoma with an aggressive extraintestinal immunohistochemical phenotype. *Sci Rep*. 2024;14(1):22241. doi:10.1038/S41598-024-72687-3
16. Sagaert X, Vanstapel A, Verbeek S. Tumor heterogeneity in colorectal cancer: what do we know so far? *Pathobiology*. 2018;85(1–2):72–84. doi:10.1159/000486721
17. Zhang Y, Zhao Y, Li Q, Wang Y. Macrophages, as a promising strategy to targeted treatment for colorectal cancer metastasis in tumor immune microenvironment. *Front Immunol*. 2021;12:685978. doi:10.3389/FIMMU.2021.685978/BIBTEX
18. Li M, He L, Zhu J, Zhang P, Liang S. Targeting tumor-associated macrophages for cancer treatment. *Cell Biosci*. 2022;12(1):1–13. doi:10.1186/S13578-022-00823-5
19. Wang H, Tian T, Zhang J. Tumor-Associated Macrophages (TAMs) in Colorectal Cancer (CRC): from mechanism to therapy and prognosis. *Int J Mol Sci*. 2021;22(16).
20. Korbelik M, Hamblin MR. The impact of macrophage-cancer cell interaction on the efficacy of photodynamic therapy. *Photochem Photobiol Sci*. 2015;14(8):1403–1409. doi:10.1039/c4pp00451e
21. Wei Y, Li R, Wang Y, Fu J, Liu J, Ma X. Nanomedicines targeting tumor cells or tumor-associated macrophages for combinatorial cancer photodynamic therapy and immunotherapy: strategies and influencing factors. *Int J Nanomed*. 2024;19:10129. doi:10.2147/IJN.S466315
22. Molecular Probes I. Qdot ITK carboxyl quantum dots; 2007. Available from: https://www.thermofisher.com/document-connect/document-connect.html?url=https://assets.thermofisher.com/TFS-Assets%2FLSG%2Fmanuals%2Fmp19020.pdf. Accessed October 19, 2024.
23. Dapkute D, Steponkiene S, Bulotiene D, Saulite L, Riekstina U, Rotomskis R. Skin-derived mesenchymal stem cells as quantum dot vehicles to tumors. *Int J Nanomed*. 2017;12:8129. doi:10.2147/IJN.S143367
24. Gollmer A, Arnbjerg J, Blaikie FH, et al. Singlet Oxygen Sensor Green®: photochemical Behavior in Solution and in a Mammalian Cell. *Photochem Photobiol*. 2011;87(3):671–679. doi:10.1111/J.1751-1097.2011.00900.X
25. Berg KCG, Eide PW, Eilertsen IA, et al. Multi-omics of 34 colorectal cancer cell lines - a resource for biomedical studies. *Mol Cancer*. 2017;16 (1):116. doi:10.1186/S12943-017-0691-Y
26. Guinney J, Dienstmann R, Wang X, et al. The consensus molecular subtypes of colorectal cancer. *Nat Med*. 2015;21(11):1350. doi:10.1038/NM.3967
27. Skripka A, Dapkute D, Valanciunaite J, Karabanovas V, Rotomskis R. Impact of quantum dot surface on complex formation with chlorin e6 and photodynamic therapy. *Nanomaterials*. 2018;9(1):9. doi:10.3390/NANO9010009
28. Perry JW, Rumi M. Two-photon absorption: an overview of measurements and principles. *Adv Opt Photonics*. 2010;2(4):451–518. doi:10.1364/AOP.2.000451
29. Bian F, Sun L, Cai L, Wang Y, Zhao Y. Quantum dots from microfluidics for nanomedical application. *Wiley Interdiscip Rev Nanomed Nanobiotechnol*. 2019;11(5). doi:10.1002/WNAN.1567
30. Soldado A, Barrio LC, Díaz-Gonzalez M, de la Escosura-Muñiz A, Costa-Fernandez JM. Advances in quantum dots as diagnostic tools. *Adv Clin Chem*. 2022;107:1–40. doi:10.1016/BS.ACC.2021.07.001
31. Jarockyte G, Poderys V, Barzda V, Karabanovas V, Rotomskis R. Blood plasma stabilized gold nanoclusters for personalized tumor theranostics. *Cancers*. 2022;14(8):1887. doi:10.3390/CANCERS14081887/S1
32. Fernandez JM, Bilgin MD, Grossweiner LI. Singlet oxygen generation by photodynamic agents. *J Photochem Photobiol B*. 1997;37(1–2):131–140. doi:10.1016/S1011-1344(96)07349-6
33. Rotomskis R, Valanciunaite J, Skripka A, et al. Complexes of functionalized quantum dots and chlorin e6 in photodynamic therapy. *Lith J Phys*. 2013;53(1):57–68. doi:10.3952/PHYSICS.V53I1.2607
34. Tsay JM, Trzoss M, Shi L, et al. Singlet oxygen production by peptide-coated quantum dot-photosensitizer conjugates. *J Am Chem Soc*. 2007;129 (21):6865–6871. doi:10.1021/JA070713I/SUPPL_FILE/JA070713ISI20070318_041803.PDF
35. Bentolila LA. Photoluminescent quantum dots in imaging, diagnostics and therapy. *Appl Nanosci Photomed*. 2015;77–104. doi:10.1533/9781908818782.77
36. Skripka A, Valanciunaite J, Dauderis G, Poderys V, Kubiliute R, Rotomskis R. Two-photon excited quantum dots as energy donors for photosensitizer chlorin e6. *J Biomed Opt*. 2013;18(7):078002. doi:10.1117/1.JBO.18.7.078002
37. Zhou Y, Lin B, Li K, et al. Preparation of near-infrared/photoacoustic dual-mode imaging and photothermal/chemo synergistic theranostic nanoparticles and their imaging and treating of hepatic carcinoma. *Front Oncol*. 2021;11:750807. doi:10.3389/FONC.2021.750807/BIBTEX
38. Yu Y, Wei D, Bing T, Wang Y, Liu C, Xiao H. A polyplatin with hands-holding near-infrared-II fluorophores and prodrugs at a precise ratio for tracking drug fate with realtime readout and treatment feedback. *Adv Mater*. 2024;36(30):2402452. doi:10.1002/ADMA.202402452
39. Qu J, Golovynska I, Liu J, Qu J, Golovynskyi S. Optical transparency windows in near-infrared and short-wave infrared for the skin, skull, and brain: fluorescence bioimaging using PbS quantum dots. *J Biophotonics*. 2024;17(11):e202400171. doi:10.1002/JBIO.202400171
40. Meiling TT, Cywiński PJ, Löhmannsröben HG. Two-photon excitation fluorescence spectroscopy of quantum dots: photophysical properties and application in bioassays. *J Phys Chem C*. 2018;122(17):9641–9647. doi:10.1021/ACS.JPCC.7B12345/SUPPL_FILE/JP7B12345_SI_001.PDF
41. Szeremeta J, Nyk M, Wawrzynczyk D, Samoc M. Wavelength dependence of nonlinear optical properties of colloidal CdS quantum dots. *Nanoscale*. 2013;5(6):2388–2393. doi:10.1039/C3NR33860F

42. Martinotti S, Ranzato E. Scratch wound healing assay. *Methods Mol Biol*. 2020;2109:225–229. doi:10.1007/7651_2019_259/COVER
43. Feng JM, Miao ZH, Jiang Y, et al. Characterization of the conversion between CD133+ and CD133- cells in colon cancer SW620 cell line. *Cancer Biol Ther*. 2012;13(14):1396. doi:10.4161/CBT.22000
44. Zhou JY, Chen M, Ma L, Wang X, Chen YG, Liu SL. Role of CD44(high)/CD133(high) HCT-116 cells in the tumorigenesis of colon cancer. *Oncotarget*. 2016;7(7):7657–7666. doi:10.18632/ONCOTARGET.7084
45. Tanaka S, Kobayashi W, Haraguchi M, Ishihata K, Nakamura N, Ozawa M. Snail1 expression in human colon cancer DLD-1 cells confers invasive properties without N-cadherin expression. *Biochem Biophys Rep*. 2016;8:120. doi:10.1016/J.BBREP.2016.08.017
46. Han S, Zong S, Shi Q, et al. Is Ep-CAM expression a diagnostic and prognostic biomarker for colorectal cancer? A systematic meta-analysis. *EBioMedicine*. 2017;20:61. doi:10.1016/J.EBIOM.2017.05.025
47. Ahmed D, Eide PW, Eilertsen IA, et al. Epigenetic and genetic features of 24 colon cancer cell lines. *Oncogenesis*. 2013;2(9):e71. doi:10.1038/ONCSIS.2013.35
48. ISO 10993-5:2009(en), Biological evaluation of medical devices — part 5: tests for in vitro cytotoxicity. Available from: https://www.iso.org/obp/ui/#iso:std:iso:10993:-5:ed-3:v1:en. Accessed November 17, 2024.
49. Guo Z, Ashrafizadeh M, Zhang W, Zou R, Sethi G, Zhang X. Molecular profile of metastasis, cell plasticity and EMT in pancreatic cancer: a pre-clinical connection to aggressiveness and drug resistance. *Cancer Metastasis Rev*. 2024;43(1):29–53. doi:10.1007/S10555-023-10125-Y
50. Sethy C, Kundu CN. 5-Fluorouracil (5-FU) resistance and the new strategy to enhance the sensitivity against cancer: implication of DNA repair inhibition. *Biomed Pharmacother*. 2021;137. doi:10.1016/J.BIOPHA.2021.111285
51. Buikhuisen JY, Torang A, Medema JP. Exploring and modelling colon cancer inter-tumour heterogeneity: opportunities and challenges. *Oncogenesis*. 2020;9(7):66. doi:10.1038/S41389-020-00250-6
52. Murciano-Goroff YR, Warner AB, Wolchok JD. The future of cancer immunotherapy: microenvironment-targeting combinations. *Cell Res*. 2020;30(6):507. doi:10.1038/S41422-020-0337-2
53. Xiong G, Huang D, Lu L, et al. Near-infrared-II light induced mild hyperthermia activate cisplatin-artemisinin nanoparticle for enhanced chemo/chemodynamic therapy and immunotherapy. *Small Methods*. 2022;6(9):2200379. doi:10.1002/SMTD.202200379
54. Mantovani A, Allavena P, Marchesi F, Garlanda C. Macrophages as tools and targets in cancer therapy. *Nat Rev Drug Discov*. 2022;21(11):799–820. doi:10.1038/s41573-022-00520-5
55. Canese R, Vurro F, Marzola P. Iron oxide nanoparticles as theranostic agents in cancer immunotherapy. *Nanomaterials*. 2021;11(8):1950. doi:10.3390/NANO11081950
56. Reichel D, Tripathi M, Perez JM. Biological effects of nanoparticles on macrophage polarization in the tumor microenvironment. *Nanotheranostics*. 2019;3(1):66. doi:10.7150/NTNO.30052
57. Miao X, Leng X, Zhang Q. The current state of nanoparticle-induced macrophage polarization and reprogramming research. *Int J Mol Sci*. 2017;18(2):336. doi:10.3390/IJMS18020336
58. Wu Y, Zhang Y, Dai LL, et al. An apoptotic body-biomimic liposome in situ upregulates anti-inflammatory macrophages for stabilization of atherosclerotic plaques. *J Control Release*. 2019;316:236–249. doi:10.1016/J.JCONREL.2019.10.043
59. Song JW, Nam HS, Ahn JW, et al. Macrophage targeted theranostic strategy for accurate detection and rapid stabilization of the inflamed high-risk plaque. *Theranostics*. 2021;11(18):8874. doi:10.7150/THNO.59759
60. Wang Q, Wang Y, Liu S, et al. Theranostic nanoplatform to target macrophages enables the inhibition of atherosclerosis progression and fluorescence imaging of plaque in ApoE(−/−) mice. *J Nanobiotechnol*. 2021;19(1):222. doi:10.1186/S12951-021-00962-W
61. Shen M, Wang Y, Bing T, Tang Y, Liu X, Yu Y. Alendronate triggered dual-cascade targeting prodrug nanoparticles for enhanced tumor penetration and STING activation of osteosarcoma. *Adv Funct Mater*. 2023;33(49):2307013. doi:10.1002/ADFM.202307013
62. Ding H, Zhang Y, Mao Y, et al. Modulation of macrophage polarization by iron-based nanoparticles. *Med Rev*. 2023;3(2):105–122. doi:10.1515/MR-2023-0002
63. Reiter I, Schwamberger G, Krammer B. Activation of macrophage tumoricidal activity by photodynamic treatment in vitro--indirect activation of macrophages by photodynamically killed tumor cells. *J Photochem Photobiol B*. 1999;50(2–3):99–107. doi:10.1016/S1011-1344(99)00078-0
64. Soyama T, Sakuragi A, Oishi D, et al. Photodynamic therapy exploiting the anti-tumor activity of mannose-conjugated chlorin e6 reduced M2-like tumor-associated macrophages. *Transl Oncol*. 2021;14(2). doi:10.1016/J.TRANON.2020.101005
65. Hayashi N, Kataoka H, Yano S, et al. A novel photodynamic therapy targeting cancer cells and tumor-associated macrophages. *Mol Cancer Ther*. 2015;14(2):452–460. doi:10.1158/1535-7163.MCT-14-0348
66. Chen X, Zheng R, Zhao L, et al. Photodynamic therapy initiated immunotherapy of self-delivery re-educator by inducing immunogenic cell death and macrophage polarization. *Chem Eng J*. 2022;435:134783. doi:10.1016/J.CEJ.2022.134783
67. Lerouge L, Gries M, Chateau A, et al. Targeting glioblastoma-associated macrophages for photodynamic therapy using AGuIX®-Design nanoparticles. *Pharmaceutics*. 2023;15(3). doi:10.3390/PHARMACEUTICS15030997